Biomacromolecules

ARTICLE

pubs.acs.org/Biomac

NMR Analysis of the Fibronectin Cell-Adhesive Sequence, Arg-Gly-Asp, in a Recombinant Silk-Like Protein and a Model Peptide

Tetsuo Asakura,*[,†] Hirohito Nishi,[†] Aya Nagano,[†,‡] Ai Yoshida,[†] Yasumoto Nakazawa,[§] Masakatsu Kamiya,[∥] and Makoto Demura[∥]

[†]Department of Biotechnology, Tokyo University of Agriculture and Technology, Koganei, Tokyo 184-8588, Japan

[‡]Research Department, Japan Medical Materials Corporation, Osaka 532-0003, Japan

[§]Nature and Science Museum, Tokyo University of Agriculture and Technology, Koganei, Tokyo 184-8588, Japan

[∥]Graduate School of Life Science, Hokkaido University, Sapporo, 060-0810, Japan

Supporting Information

ABSTRACT: It is well established that by introducing the cell-adhesive sequence Arg-Gly-Asp (RGD) from fibronectin into *Bombyx mori* silk fibroin by covalent coupling or bioengineering techniques, excellent biomaterials have been developed with the modified silk fibroin. However, there is no report about the structure and dynamics of the RGD moiety in the silk fibroin. To clarify the origin of such a high cell adhesion character and to design new recombinant silk protein with higher cell adhesion ability, it is necessary to characterize the structure and dynamics of the RGD moiety introduced into silk fibroin. In this study, the structure and dynamics of the RGD moiety in a recombinant silk-like protein, $SLPF_{10}$, consisting of the repeated silk fibroin sequence $(AGSGAG)_3$ and the sequence ASTGRGDSPA including the RGD moiety, were studied using solution NMR. The ^{1}H, ^{15}N, and ^{13}C chemical shifts indicate that the RGD moiety, as well as the silk fibroin sequence, takes a random coil form with high mobility in aqueous solution. Next, a ^{13}C solid-state NMR study was performed on a ^{13}C selectively labeled model peptide, AGSGAG[3-^{13}C]A^{7}GSGAGAGSGGT[2-^{13}C]G^{19}R[1-^{13}C]G^{21}DSPAG-GGAGAGSGAG. After formic acid treatment, an increase in the β-sheet fraction for the AGSGAG sequence and peak narrowing of the residues around the RGD moiety were observed in the dry state. The latter indicates a decrease in the chemical shift distribution although the RGD moiety is still in random coil. A decrease in the peak intensities of the RGD moiety in the swollen state after immersing it in distilled water was observed, indicating high mobility of the RGD sequence in the peptide in the swollen state. Thus, the random coil state of the RGD moiety in the recombinant silk-like protein is maintained in aqueous solution and also in both dry and swollen state. This is similar to the case of the RGD moiety in fibronectin. The presence of the linker ASTG at the N-terminus and SPAGG at the C-terminus seems important to maintain the random coil form and the flexible state of the RGD sequence in order to permit access for binding to various integrins.

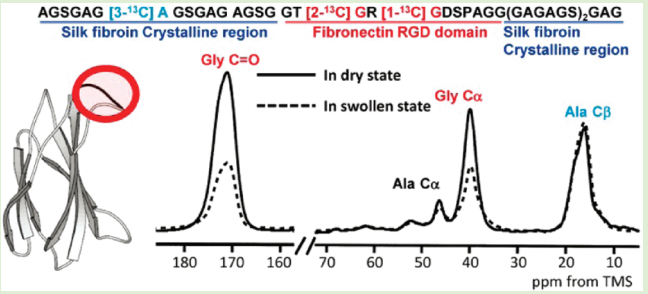

INTRODUCTION

Silks are generally defined as fibrous proteins that are spun into fibers by some lepidoptera larvae such as silkworms, spiders, scorpions, mites and flies.[1] Silk fiber has a long history of use in textiles. Recently, silk fibroin from *Bombyx mori* (*B. mori*) has been reported to have many inherently superior properties as biomaterials, in terms of mechanical properties, environmental stability, biocompatibility, low immunogenicity, and biodegradability.[2−10] In addition, by introducing the cell-adhesive sequence Arg-Gly-Asp (RGD) from fibronectin into the silk fibroin by covalent coupling or bioengineering techniques, better biomaterials have been developed with the modified silk fibroin because of the ability of RGD to promote cell attachment.[11] In fact, recombinant silk fibroin containing RGD in the primary sequence after cloning and expression from *Escherichia coli* is now available as commercial products, for example, Pronectin F.[12]

Research carried out in Kaplan's group emphasized the potential of the RGD-coupled silk fibroin in tissue engineering. For example, silk fibroins coupled with RGD increased osteoblast-like cell adhesion and expression of both alkaline phosphatase and osteocalcin compared with those without RGD.[2] The RGD-coupled silk fibroins can also support human bone marrow stromal cell attachment and are suitable for autologous bone tissue engineering.[13−15] RGD-coupled silk protein-biomaterial lamellar systems were also used for corneal tissue engineering.[16]

In our previous studies,[17−20] we designed and produced several recombinant silk proteins containing the repeated sequences of RGD within the longer sequences, ASTGRGDSPA,

Received: June 26, 2011
Revised: September 22, 2011
Published: September 28, 2011

by expression in *E. coli*. The other parts of the repeated sequences in the proteins were the crystalline regions of several silk fibroins: $(AGSGAG)_3$ from *B. mori*,[19] A_{12} from *Samia cynthia ricini*,[18] and $(AG)_9$ or $(AAG)_6$ from *Anaphe*[20] together with a part of elastin $(GVPGV)_2$ and *B. mori* silk fibroin $(AGSGAG)_3$.[19] Recombinant silk films prepared on a plastic plate by cell culture or recombinant silk fibers after electrospinning were used for cell-adhesive experiments with NHDF or VERO cells. In addition, we constructed transgenic silkworms, inserting modified fibroin light-chain genes for making recombinant silks containing RGD.[21,22] In all cases, remarkably higher cell adhesion activities were obtained for the recombinant silk fibroin compared with natural silk fibroin without RGD.

To clarify the origin of such a high cell adhesion character and to design new recombinant silk protein with higher cell adhesion ability, it is necessary to characterize the structure and dynamics of the RGD moiety introduced into silk fibroin. To date, no details have been reported. NMR is a very powerful technique for this purpose. Solution NMR coupled with ^{15}N and $^{13}C/^{15}N$ labeling has been used to study the structural significance of module−module interactions in the RGD-dependent cell binding region of human fibronectin, comprising the 9th and 10th fibronection type III, by Campbell's group.[23] NMR chemical shifts and ^{15}N relaxation data together with equilibrium and kinetic unfolding experiments have shown nonspecific protein−protein interactions which provide the bulk of the thermodynamic stabilization and the motional constraint between the two modules. T_2 spin−spin relaxation times of ^{15}N nuclei in the F−G loop in the human fibronectin type III module which contains the RGD sequence are significantly longer relative to the overall T_2, indicating that this loop is highly flexible. Copie et al.[24] have also reported the solution structure of the mouse fibronectin cell attachment domain consisting of the linked 9th and 10th type II modules. The 10th module contains the RGD cell attachment sequence while the 9th contains the synergy region, which has the cell attachment activity of intact fibronectin. The NMR results suggest that the two modules form a less extended and more flexible structure than the fully extended rod-like crystal structure. The relaxation parameters indicate that several loops in this domain including the RGD loop are flexible on the nanosecond to picosecond timescale in solution. Thus, the RGD sequence in fibronectin is flexible and exists as random coil with high cell attachment activity.

Because silk modified with RGD is usually used in both dry and swollen states as a scaffold for biomaterials, it is necessary to obtain information on the RGD moiety in the dry and swollen states. NMR studies of modified silks are not straightforward because of the presence of the His-tag in $SLPF_{10}$ and peak broadening in the solid state. For this purpose, solid-state NMR coupled with selective stable isotope labeling is useful. Earlier we have already reported detailed studies of the structure of the silk fibroin using several solid-state NMR techniques and appropriate model peptides with selective stable isotope labeling. The conformation-dependent ^{13}C chemical shifts in the solid state were used effectively to distinguish two crystalline forms of *B. mori* silk fibroin, Silk I and Silk II.[25,26] By adding other solid-state NMR techniques such as REDOR or spin-diffusion NMR to the chemical shift information, the Silk I structure of *B. mori* silk fibroin before spinning was clarified to be a repeated type-II β-turn in the solid state.[27−29] The structure after spinning, which is now Silk II, was found to be heterogeneous.[30,31] This structure was determined to contain about 70% antiparallel β-sheet, and 30% distorted β-turn and/or random coil, based on the Ala Cβ line shape in the ^{13}C CP/MAS NMR spectra of the crystalline region of *B. mori* silk fibroin in Silk II form. The antiparallel β-sheet region can also be divided further into two forms with different intermolecular arrangement. Thus, it has been shown that solid-state NMR coupled with the use of the appropriate model peptides and selective stable isotope labeling is very useful for structural analysis in the solid state.

In this paper, we obtain structural and dynamic information on the RGD moiety in the recombinant silk protein $SLPF_{10}$ consisting of repeated $(AGSGAG)_3$ and the sequence ASTGRGDSPAGG. For comparison, the structure of repeated TGRGDSPAAS sequences, RGD_8, was also analyzed. We used at first solution NMR coupled with ^{15}N and $^{13}C/^{15}N$ labeling. Conformation-dependent chemical shifts are used to probe the local conformation of the RGD-containing sequence ASTGRGDSPAGG in aqueous solution. Next, solid-state NMR was used for getting information on the structure of the RGD moiety and silk fibroin sequence in dry and swollen states before and after formic acid treatment to induce Silk II formation. A solid-state NMR study was performed on the model peptide, AGSGAG[3-^{13}C]A^7GSGAGAGSGGT[2-^{13}C]G^{19}R[1-^{13}C]-G^{21}DSPAGGGAGAGSGAG, in dry and swollen states. Here, [3-^{13}C]A^7 labeling gives information on the silk fibroin part and the two Gly labelings, [2-^{13}C]G^{19} and [1-^{13}C]G^{21}, information on the RGD moiety. Dynamic information on the RGD moiety in the swollen state in silk-like proteins was also obtained indirectly using solid-state NMR through changes in the effectiveness of $^{13}C-^{1}H$ cross-polarization (CP).[19,20,32]

MATERIALS AND METHODS

1. Production of Proteins. Two recombinant proteins, $SLPF_{10}$ and RGD_8, were used for NMR observation. The primary structure of $SLPF_{10}$ is MHHHHHHSSGLVPRGSGMKETAAAKFERQHMDS-PDLGTDDDDKAMADIGSSRTS[TGRGDSPAGG(GAGAGS)$_3$AS]$_{10}$MSRVDLKLAAALEHHHHHH and that of RGD_8 is MHH-HHHHSSGLVPRGSGMKETAAAKFERQHMDSPDLGTDD-DDKAMADIGSSRTS(TGRGDS-PAAS)$_8$MSRVDLKLAAAL-EHHHHHH. Details on the preparations of $SLPF_{10}$ and RGD_8 were reported previously.[19,22] In this paper, larger-scale cultivation by *E. coli* was performed in a 2.4-L TB medium using a fermenter (Marubishi Bio Eng., Japan), and expression of the recombinant proteins was induced with IPTG. The proteins were purified with nickel-chelate chromatography, and identified by SDS−PAGE.

2. Stable-Isotope Labeling of Proteins. For solution NMR analysis, uniformly ^{15}N- and $^{13}C/^{15}N$-labeled $SLPF_{10}$ and RGD_8 were expressed as His-tagged protein from *E. coli* BL21(DE3)pLysS in ^{15}N-rich or ^{15}N- and ^{13}C-rich CHL (Shoko Co., Ltd., Japan) medium and purified by Ni^{2+} column, followed by gel filtration chromatography.

3. Peptide Synthesis. The peptides $(AGSGAG)_5$ and $(AG)_{15}$ were prepared as model peptides for the crystalline region of *B. mori* silk fibroin as reported previously.[27−31,33] The peptide $(AGSGAG)_2$AG-SGGTGRGDSPAGGGAG$(AGSGAG)_2$ and ^{13}C selectively labeled peptide AGSGAG[3-^{13}C]A^7GSGAGAGSGGT[2-^{13}C]G^{19}R[1-^{13}C]G^{21}-DSPAGGGAGAGSGAG were prepared as models of the silk-like protein, $SLPF_{10}$. The TGRGDSPAG sequence was inserted by adding a GG unit at the N- and C-terminal ends of this model peptide into the crystalline region of *B. mori* silk fibroin. These model peptides were synthesized by the F-moc solid phase method. A fully automated Pioneer Peptide Synthesis System (Applied Biosystems Ltd.) was used throughout. The crude peptides were purified by RP-HPLC using 0.1% TFA-H_2O and 0.08%TFA-acetonitrile as eluent. After purification,

acetonitrile was removed by evaporation and then aqueous solutions of the peptides were lyophilized for 24 h. The lyophilized peptides were dissolved in aqueous solution and the pH was adjusted to 10.6. The peptides were also dissolved in formic acid (FA) and then air-dried to produce Silk II (Treatment: FA).[30,31]

4. Cell Adhesion Inhibition Assay. The osteoblast cell adhesion activities of $SLPF_{10}$ and RGD_8 in aqueous solution were examined using an assay to monitor the inhibition of cell-spreading of osteoblast-like cell line MC3T3-E1 (RIKEN, Japan). This assay is routinely used to determine the biological activity of proteins containing cell binding motifs. The 96-well tissue culture plates (Falcon, U.K.) were preincubated with 50 μL of 25 μg/mL human plasma fibronectin (Sigma-Aldrich, Japan). Free binding sites on the plastic were blocked with 1% bovine serum albumin (BSA)/phosphate buffered saline (PBS) (100 μL/well) for 1 h at 37 °C. Fibronectin/BSA-only coated wells were used as standard. MC3T3-E1 cells (3000 cells/well) in 100 μL of α-minimal essential medium (MEM) supplemented with 10% fetal bovine serum (FBS) were added to each well, with 25 μL of protein solution in phosphate-buffered saline. After 2 h incubation at 37 °C in a 5% CO_2 atmosphere, unattached cells were removed by gently rinsing the wells twice with warm PBS. Attached cells were fixed with 2% paraformaldehyde in PBS (100 μL/well) and stained with DAPI solution (0.005 mg/mL) in PBS (100 μL/well). After 5-min incubation at room temperature, stained cells were counted using a fluorescence microscope with appropriate filters. The reported results are the mean values of triplicate determinations.

5. Cell Adhesion Assay on Tissue Culture Plate. The osteoblast cell adhesion activities of silk fibroin and $SLPF_{10}$ were examined in 96-well tissue culture plates. The samples were dissolved in FA (concentration 10% w/v) and then pipetted onto the plate. To remove FA, the plate was dried in air for 12 h, then incubated in 50% methanol for 10 min and dried in air for 12 h again. It was also attempted to use RGD_8 to coat the plate in a similar manner. However, the coated RGD_8 was still soluble in water, and therefore, these experiments were unsuccessful. The osteoblast cell adhesion activities of silk fibroin and $SLPF_{10}$ on the plate were determined using MC3T3-E1. The protein amount was 0.4 mg/cm^2. The number of cultured cells was 3000 cells/well. After 2 h incubation at 37 °C in a 5% CO_2 atmosphere, the attached cells were fixed with 2% paraformaldehyde in PBS and stained with DAPI solution in PBS. After 5 min incubation at room temperature, stained cells were counted using a fluorescence microscope with appropriate filters. The reported results are the mean values of triplicate determinations.

6. Solution NMR Measurements. NMR spectra were recorded for purified recombinant silk proteins dissolved in 50 mM phosphate-Na (pH 4.0 and pH 7.0), 50 mM EDTA, and 10% ^2H_2O. The protein solutions were concentrated to 0.3−0.5 mM with an Amicon Ultra device (Millipore, Bedford, MA). All NMR spectra were acquired at 30 °C on a Bruker DMX 500 spectrometer equipped with cryoprobe and a JEOL ECX-400 spectrometer. ^1H, ^{13}C, and ^{15}N sequential assignments were obtained using two-dimensional (2D) and three-dimensional (3D) heteronuclear NMR experiments: 2D $^1H-^{15}N$ HSQC, 2D $^1H-^{13}C$ HSQC, 3D HNCO, 3D CBCA- (CO)NH, 3D HNCA, 3D HNHB, HN(CO)CA, and 3D-HN(CA)NH. The spectra were processed using NMR Pipe software[34] and analyzed using SPARKY 3 software .[35]

7. Solid-State NMR Measurements. ^{13}C CP/MAS NMR experiments were performed on a Chemagnetics Infinity 400 spectrometer and a Bruker DSX-400 AVANCE spectrometer with an operating frequency of 100.0 MHz for ^{13}C at a sample spinning rate of 8 kHz in a 4 mm diameter ZrO_2 rotor. The ^1H 90° pulse was 3 μs and a 70 kHz rf field was used during CP and decoupling. A total of 10−20K scans for the nonlabeled sample were collected over a spectral width of 35 kHz with a recycle delay of 3 s. All spectra were obtained using a CP contact time of 2 ms and TPPM decoupling. The line broadening was 20 Hz. ^{13}C chemical shifts were calibrated indirectly using the adamantane methine peak observed at 28.8 ppm relative to TMS (tetramethylsilane) at 0 ppm. For preparation of the sample in the swollen state, the peptide powder was first immersed in distilled water for 2 h and then transferred to a sample tube. The tube was sealed using epoxy resin glue and allowed to stand for one day before NMR observation.

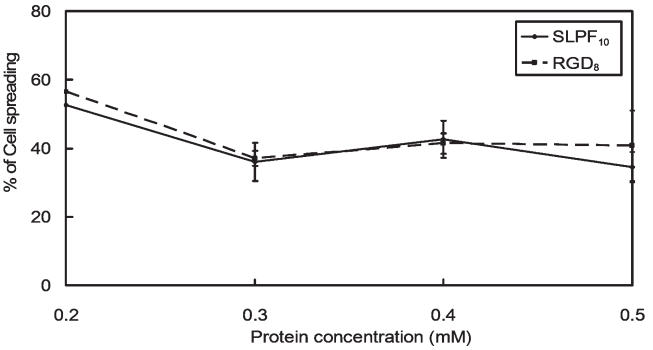

Figure 1. Inhibition effects of cell-spreading of the osteoblast-like cell MC3T3-E1 by $SLPF_{10}$ and RGD_8 in aqueous solution. Details are described in the text.

RESULTS AND DISCUSSION

1. Cell Adhesion Activities of $SLPF_{10}$ and RGD_8 in Aqueous Solution. The osteoblast cell adhesion activities of $SLPF_{10}$ and RGD_8 in aqueous solution were examined because the solution structure of the RGD moiety in the two proteins is compared in the next section. In this way, the correlation between the activity and structure is examined. For this purpose, the ability of $SLPF_{10}$ and RGD_8 to inhibit cell adhesion was examined. MC3T3-E1 cells were plated on fibronectin. Both $SLPF_{10}$ and RGD_8 inhibited about 40% of the MC3T3-E1 cell adhesion to fibronectin at a concentration of 0.5 mM (Figure 1). Thus, these experiments demonstrate that $SLPF_{10}$ and RGD_8 are promising inhibitors of MC3T3-E1 cell adhesion. There was no significant difference between the two proteins within the limits of experimental error.

2. Solution NMR. The conformations of $SLPF_{10}$ and RGD_8 in aqueous solution were studied by solution NMR. The ^1H, ^{15}N, and ^{13}C NMR spectra were assigned by combination of $^1H-^{15}N$ HSQC, $^1H-^{13}C$ HSQC, CBCANH, CBCA(CO)NH, HNCA, HN(CO)CA, HNCO, and HN(CA)CO.

Figure 2a shows a $^1H-^{15}N$ HSQC spectrum of $SLPF_{10}$ in aqueous solution together with the peak assignments. The sequential assignments were performed only for the residues within the repeated sequence in $SLPF_{10}$, which have identical shifts within each repeat because of peak overlap. In general, the ^{15}N chemical shift is affected largely by the amino acid at the N-terminal side of the given amino acid, but also by the local conformation around the ^{15}N nucleus.[36,37] The observation of the same chemical shifts for the sets of Gly,[13,15,19,21,34,36] Ala,[12,14,18,20,33,35] and Ser[16,22,37] residues indicates that the AGSGAG region in $SLPF_{10}$ is in a similar chemical environment for each repeat and, thus, that the local conformation is the same for each repeated sequence. In addition, judging from the ^{15}N and ^1HN chemical shifts of these peaks, it is suggested that the AGSGAG region is in the form of random coil.[37−40] The chemical shift values are summarized together with the line widths in Table 1 of the Supporting Information. From the chemical shifts, the $R^3G^4D^5$ moiety is also in the random coil

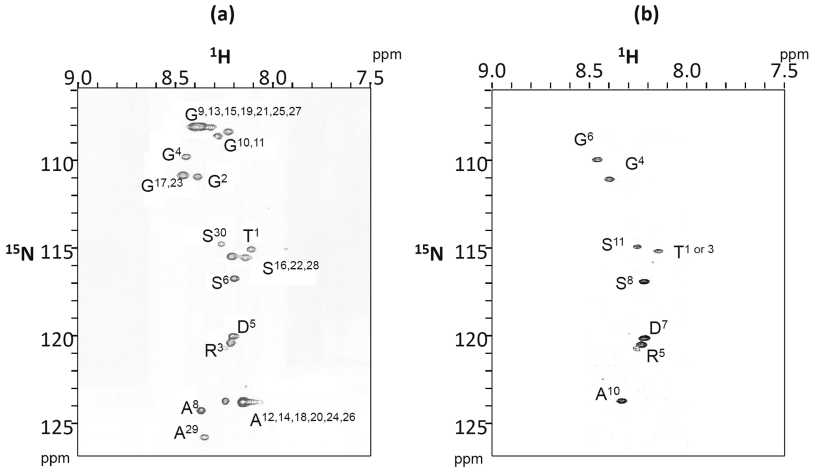

Figure 2. ^{1}H−^{15}N HSQC spectra of (a) $SLPF_{10}$, which consists mainly of the repeated sequence $(T^1G^2R^3G^4D^5S^6P^7A^8G^9G^{10}G^{11}A^{12}G^{13}A^{14}G^{15}S^{16}G^{17}A^{18}G^{19}A^{20}G^{21}S^{22}G^{23}A^{24}G^{25}A^{26}G^{27}S^{28}A^{29}S^{30})_{10}$ and (b) RGD_8, which contains the repeated sequence $(T^1S^2T^3G^4R^5G^6D^7S^8P^9A^{10}S^{11})_8$, in aqueous solution together with the peak assignments. Only the parts of the repeated sequences in both proteins are shown. The P peak could not be observed because there is no NH proton. The S^2 peak in (b) seems to be overlapped with other S peaks. The ^{1}HN and ^{15}N chemical shift values are summarized in Table 1 of the Supporting Information together with ^{13}C chemical shift values.

region. Thus, the RGD part in $SLPF_{10}$ has a random coil conformation when the AGSGAG region is in the random coil form.

Figure 2b shows the ^{1}H−^{15}N HSQC spectrum of RGD_8 in aqueous solution and the chemical shifts are also listed in Table 1 of the Supporting Information. Thus, the chemical environment can be compared between the cell-adhesive RGD parts in $SLPF_{10}$ and RGD_8 through the chemical shifts. The ^{15}N chemical shifts of the six residues of the sequence TGRGDS in $SLPF_{10}$ and RGD_8 are in agreement with each other within less than 0.1 ppm. Similarly, the NH proton chemical shifts are also in agreement within 0.02 ppm. In particular, the NH proton chemical shifts are sensitive to the spatial environment through C−N or C═O bond anisotropy effects,[38] and therefore, the local conformation of the sequence TGRGDS in $SLPF_{10}$ and RGD_8 is concluded to be the same. The chemical shifts of the $^{13}C\alpha$ carbons, which are also sensitive to the conformation, are also the same as listed in Table 1 of the Supporting Information. Thus, in view of the conformation-dependent chemical shift,[38−40] TGRGDSPA together with silk fibroin sequence is in random coil for both proteins. Both proteins are also in a highly mobile state judging from the narrow line widths listed in Table 1 of the Supporting Information. The RGD loop in both proteins can therefore adjust to accommodate variations in integrin structure or other environments due to its high flexibility in both proteins. In turn, no effect has been seen of the presence of the sequences of *B. mori* silk fibroin $(AGSGAG)_3$ adjacent to the RGD unit at both N- and C-sites in $SLPF_{10}$ on cell adhesion in aqueous solution. Thus, the proteins $SLPF_{10}$ and RGD_8 are promising inhibitors of MC3T3-E1 cell adhesion and there was no significant difference between the two proteins.

3. Cell Adhesion Assays of $SLPF_{10}$ and RGD_8 in the Solid State. The osteoblast cell adhesion activities of silk fibroin and $SLPF_{10}$ were examined on 96-well tissue culture plates in order to obtain further information on the RGD moiety in dry and swollen states which is usually used as a scaffold. It was also attempted to use RGD_8 to coat the plate with FA, but the coated RGD_8 was still soluble in water, making measurements impossible. The observed cell adhesion activities on silk fibroin coated and $SLPF_{10}$ coated plates are shown in Figure 3 as histograms relative to untreated plates. The activity of $SLPF_{10}$ was significantly higher than that of the parent protein, *B. mori* silk fibroin without RGD sequence. The experimental error for $SLPF_{10}$ is relatively large compared with that of silk fibroin. This is due to the fact that the $SLPF_{10}$ film tends to be slightly heterogeneous compared with silk fibroin. However, it is clear that high cell adhesion activity was obtained by introducing the cell-adhesive sequence RGD into the silk fibroin.

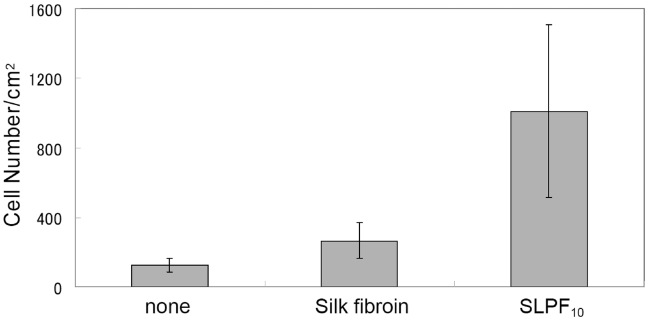

Figure 3. Histograms showing the numbers of adhered MC3T3-E1 cells after 2 h cultivation on untreated plates (none), plates coated by *B. mori* silk fibroin without RGD (silk fibroin), and with RGD ($SLPF_{10}$). Details are described in the text.

4. ^{13}C CP/MAS NMR Spectra of Nonlabeled Peptides. The structure of the silk fibroin sequence and the RGD moiety in $SLPF_{10}$ must also be examined in the solid state with solid-state NMR because the recombinant silk protein is usually used as a scaffold. However, it was difficult to obtain such information clearly because of the presence of the His-tag in $SLPF_{10}$ and peak broadening. Therefore, we synthesized a model peptide for $SLPF_{10}$, $(AGSGAG)_2$-AGSGGTGRGDSPAGGGAG$(AGSGAG)_2$.

Figure 4 shows the ^{13}C CP/MAS NMR spectra of $(AG)_{15}$, $(AGSGAG)_5$, and the model peptide of $SLPF_{10}$ in the solid state. These peptides were observed after dialysis of 9 M LiBr aqueous solutions. Conformation-dependent ^{13}C chemical shifts in the solid state can be used to distinguish clearly between Silk I and

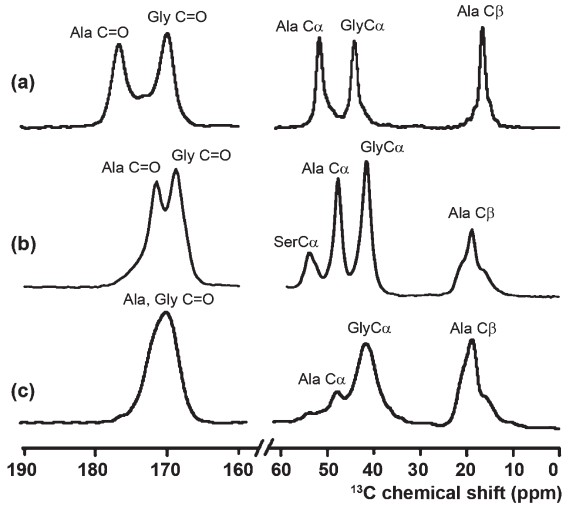

Figure 4. ^{13}C CP/MAS NMR spectra of (a) $(AG)_{15}$, (b) $(AGSGAG)_5$, and (c) $SLPF_{10}$ in the solid state. These peptides were observed after dialysis of 9 M LiBr aqueous solutions. From the chemical shift and the line shape of Ala Cβ carbons, the conformation is Silk I in (a), and Silk II for (b) and (c).

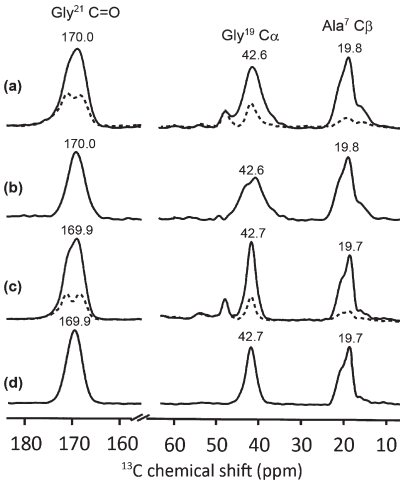

Figure 5. ^{13}C CP/MAS NMR spectra of (a) ^{13}C labeled peptide, AGSGAG[3-^{13}C]A^{7}GSGAGAGS-GGT[2-^{13}C]G^{19}R[1-^{13}C]G^{21}DSP-AGGGAGAGSGAG (solid line) and nonlabeled peptide (broken line). By subtracting the spectrum of nonlabeled peptide from that of the ^{13}C selectively labeled peptide, the difference spectrum (b) was obtained. Similarly, ^{13}C CP/MAS NMR spectra were observed after formic acid treatment and are shown in (c), producing the difference spectrum (d).

Silk II.[25−31] A sharp peak at 16.7 ppm in the Ala Cβ region, together with a sharp peak for Ala Cα (50.7 ppm) and Ala carbonyl carbons (176.8 ppm), indicates Silk I form. Two peaks observed at 19.6 and 22.2 ppm, together with a broad peak at 16.7 ppm in the Ala Cβ region, can be assigned to Silk II form of *B. mori* silk fibroin. The 22.2 ppm peak is assigned to a conformation in which all methyl groups of Ala residues point in the same direction, whereas the 19.6 ppm peak comes from a conformation in which the methyl groups alternately point in opposite directions in adjacent sheets.[31] Thus, the conformation is Silk I for $(AG)_{15}$ because of the sharp peak at 16.7 ppm observed for the Ala Cβ carbon, and that of $(AGSGAG)_5$ is Silk II judging from the asymmetric Ala Cβ peak at around 20 ppm.

In our previous paper,[33] we reported that the presence of the Ser residue in the sequence AGSGAG has a role in changing the structure from Silk I to Silk II in the crystalline region of *B. mori* silk fibroin after dialysis of a 9 M LiBr solution against distilled water. The structure of the model peptide of $SLPF_{10}$ is basically Silk II judging from the asymmetric Ala Cβ peak at around 20 ppm, although the line shape is slightly different from that of $(AGSGAG)_5$. Thus, the characteristic of the AGSGAG sequence including the role of the Ser residue seems to be maintained even if the sequence, TGRGDSPA, is inserted at the center of the model peptide. Thus, the repeated AGSGAG sequences have a strong propensity to form β-sheet structure. The Gly Cα peak of the model peptide of $SLPF_{10}$ is slightly broader than that of $(AGSGAG)_5$, but it is difficult to discuss the structure in detail from these spectra including the RGD moiety because of a mixture of several Gly peaks in the model peptide. Therefore, selective ^{13}C isotope labeling of the model peptide of $SLPF_{10}$ was performed and is discussed in the next section.

5. ^{13}C CP/MAS NMR Spectra of ^{13}C Labeled Model Peptides of $SLPF_{10}$. The ^{13}C selectively labeled model peptide of $SLPF_{10}$, AGSGAG[3-^{13}C]A^{7}GSGAGAGSGGT[2-^{13}C]G^{19}-R[1-^{13}C]G^{21}DSPAGGGAGAGSGAGAGSGAG was synthesized. A more detailed structural analysis was performed by subtracting the nonlabeled spectrum (broken line) from the ^{13}C selectively labeled spectrum shown in Figure 5a. The difference spectrum is shown in Figure 5b. The ^{13}Cβ labeling of A^7 provides structural information on the surrounding sequence, $(AGSGAG)_2$, in the solid state.[34] The line shape of the Ala ^{13}Cβ peak (Figure 5a) is similar to that of the Ala Cβ peak of the nonlabeled peptide (Figure 4c), implying that each Ala residue in the peptide adopts a similar β-sheet structure. As shown in Figure 5c after treatment of FA which was applied to prepare Silk II structure, the broad component at the upfield side of the ^{13}Cβ peak of Ala^7 residue decreases in intensity, indicating that the random coil component has largely changed to β-sheet due to the FA treatment.

^{13}C labeling of Gly C$^{\alpha}$ and CO carbons in the sequence [2-^{13}C]G^{19}R[1-^{13}C]G^{21}D^{22} also gives local structural information on the RGD sequence located in the center of the peptide, although the range of the conformation-dependent Gly chemical shift is relatively small compared with that of Ala.[40] A chemical shift of 170 ppm was observed for the G^{21} residue, indicating that G^{21} assumes a random coil form, although the line width decreased by 10% after treatment with FA. The most remarkable change with FA treatment was observed for the Cα carbon of G^{19}. The chemical shift of the peak center, 42.7 ppm, is basically the same before and after FA treatment; however, the line width is quite different (Figure 5). Since the label is specific to G^{19}, the broadening does not originate from overlapping resonances due to multiple Gly residues. Thus, the broadening means that the G^{19} residue takes on many conformations with different torsion angles.[40] After FA treatment, the number of conformations decreases, although the structure is still random coil in the solid state.

A deconvolution of the Ala^7 Cβ peak in the difference spectra (Figure 5b,d) is shown in Figure 6 together with the fraction (%) of each conformation. The assignment of the Ala Cβ peak of *B. mori* silk fibroin and their model peptides has been reported previously.[30,31] The two peaks observed at 19.6 and 22.2 ppm together with the broad peak at 16.7 ppm in the Ala Cβ region can be assigned to the Silk II form of *B. mori* silk fibroin. The 22.2 ppm peak can be assigned to a conformation in which all methyl groups of Ala residues point in the same direction,

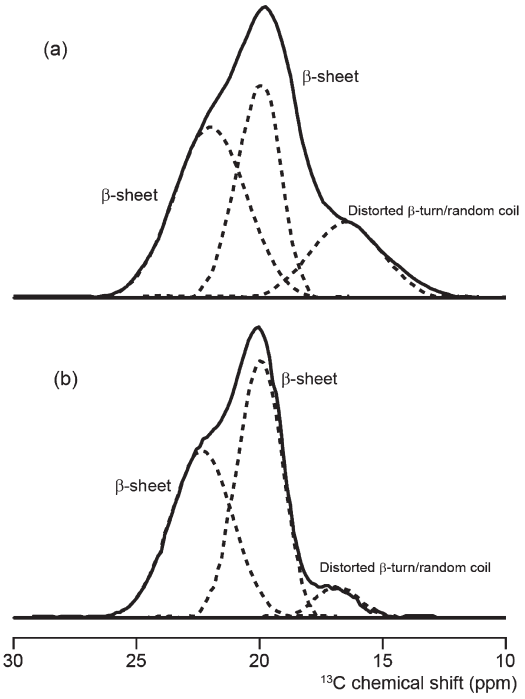

Figure 6. Decompositions of the Ala Cβ peaks of the ^{13}C labeled peptide shown in Figure 5, (a) before and (b) after formic acid treatments by assuming Gaussian line shape.

whereas the 19.6 ppm peak derives from a conformation in which the methyl groups point alternately in opposite directions in the adjacent sheets. Before FA treatment (Figure 6a), the fraction of antiparallel β-sheet at 22.2 ppm was determined to be 41%, the fraction of antiparallel β-sheet at 19.6 ppm to be 37%, and the fraction in the distorted β-turn and/or random coil at 16.7 ppm was 22%. Thus, in spite of the presence of the cell-adhesive sequence TGRGDSPA in the molecule, the repeated AGSGAG sequence at the N- and C-terminal sites tends to form antiparallel β-sheet structure. After FA treatment (Figure 6b), the fraction of the upfield component decreases from 22% to 7%. On the other hand, the fraction of the center peak at 19.6 ppm increases from 37% to 49%. Thus, a conformational transition from random coil to β-sheet in the repeated AGSGAG sequences occurs on FA treatment, although the fraction of the downfield peak is almost the same (41% before FA treatment and 44% after FA treatment). The local structure of the RGD part is still random-coil after FA treatment, but the number of the conformations with different torsion angles decreases as evidenced by the peak narrowing.[40]

6. ^{13}C CP/MAS NMR Spectra of Labeled Peptides under Wet Conditions. The ^{13}C labeled model peptide of $SLPF_{10}$ after FA treatment was observed with solid-state NMR under the swollen conditions in order to reproduce the cell-adhesion experiment. Thus, $SLPF_{10}$ was coated onto the plate during its cultivation in the aqueous solution. Figure 7 shows ^{13}C CP/MAS NMR spectra of the model peptide in dry (solid line) and swollen states (broken line). The peak intensities of the Cα carbon of the Gly residue just before the RGD sequence and the CO carbon of the Gly residue in the RGD sequence of TGRGDSPA decreased remarkably, although that of Ala Cβ in the AGSGAG region did not change. These results indicate that the CP effect from ^{1}H to ^{13}C nuclei is not effective because of the high mobility in the TGRGDSPA region in the swollen state.[32] This indicates that the

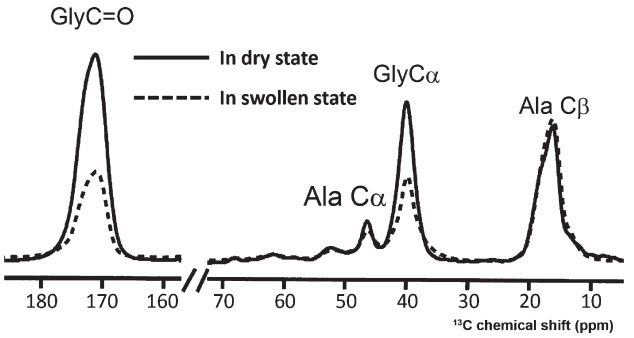

Figure 7. ^{13}C CP/MAS NMR spectra of the ^{13}C labeled peptide, AGSGAG[3-^{13}C]A^{7}GSGAGAGSGGT-[2-^{13}C]G^{19}R[1-^{13}C]G^{21}DSP-AGGGAGAGSGAG shown in Figure 5 in dry state (solid line) and in swollen state (broken line).

RGD is in flexible and mobile states, which provides an explanation for how the activity can be still high as in aqueous solution. In contrast, the line shape of the Ala^{7}Cβ peak in the sequence AGSGAG does not change and still indicates β-sheet conformation. The repeated sequence of AGSGAG in antiparallel β sheet conformation is considered to be adsorbed onto the plate by hydrophobic interaction which is not affected by the water in the swollen state. However, the region TGRGDSPA is in random coil conformation with high mobility in the swollen state as well as in aqueous solution. Thus, the cell-adhesive activity is still maintained.

CONCLUSION

Since there is no report about the structure and dynamics of the RGD moiety introduced into recombinant silk-like proteins, we obtained such information using both solution and solid-state NMR.

The RGD moiety takes a random coil form and is in a highly mobile state in aqueous solution. A ^{13}C solid-state NMR study on the ^{13}C selectively labeled model peptide indicates that random coil state of the RGD moiety is maintained in aqueous solution and also in both dry and swollen state. This is similar to the case of the RGD moiety in fibronectin. The presence of the linker ASTG at the N-terminus and SPAGG at the C-terminus seems important to maintain the random coil form and the flexible state of the RGD sequence in order to permit access for binding to various integrins.

ASSOCIATED CONTENT

Supporting Information. Information on the chemical shifts of each amino acid residue. This material is available free of charge via the Internet at http://pubs.acs.org.

AUTHOR INFORMATION

Corresponding Author
*Tel: (+81) 423837733. E-mail: asakura@cc.tuat.ac.jp.

ACKNOWLEDGMENT

T.A. acknowledges support by grant from the Ministry of Agriculture, Forestry and Fisheries of Japan (Agri-Health Translational Research Project) and support from a Grant-in-Aid for Scientific Research from Ministry of Education, Science, Culture and Supports of Japan (23245045) and (23500512). We would

like to thank Dr. Heisaburo Shindo for giving useful advice and comments. In addition, we are grateful to Prof. Mike Williamson (University of Sheffield, U.K.) for careful reading and checking of the manuscript.

REFERENCES

(1) Asakura, T.; Kaplan, D. L. Silk production and processing. In *Encyclopedia of Agricultural Science*; Arutzen, C. J., Ed.; Academic Press: San Diego, CA, 1994; Vol. 4, pp 1−11.
(2) Sofia, S.; McCarthy, M. B.; Gronowicz, G.; Kaplan, D. L. *J. Biomed. Mater. Res.* **2001**, *54*, 139–148.
(3) Altman, G. H.; Diaz, F.; Jakuba, C.; Calabro, T.; Horan, R. L.; Chen, J.; Lu, H.; Richmond, J.; Kaplan, D. L. *Biomaterials* **2003**, *24*, 401–416.
(4) Vepari, C.; Kaplan, D. L. *Prog. Polym. Sci.* **2007**, *32*, 991–1007.
(5) Numata, K.; Kaplan, D. L. *Adv. Drug Delivery Rev.* **2010**, *62*, 1497–1508.
(6) Kuzuhara, A.; Asakura, T.; Tomoda, R.; Matsunaga, T. *J. Biotechnol.* **1987**, *5*, 199–207.
(7) Demura, M.; Asakura, T. *Biotechnol. Bioeng.* **1989**, *33*, 598–603.
(8) Makaya, K.; Terada, S.; Ohgo, K.; Asakura, T. *J. Biosci. Bioeng.* **2009**, *108*, 68–75.
(9) Enomoto, S.; Sumi, M.; Kajimoto, K.; Nakagawa, Y.; Takahashi, R.; Takabayashi, C.; Asakura, T.; Sata, M. *J. Vasc. Surg.* **2010**, *51*, 155–164.
(10) Asakura, T.; Koyanagi, R.; Nishiyama, N.; Kuboyama, N.; Kiba, H.; Abiko, Y. *J. Insect Biotech. Sericol.* **2011**, *80*, 25–30.
(11) Hersel, U.; Dahmen, C.; Kessler, H. *Biomaterials* **2003**, *24*, 4385–4415.
(12) Cappello, J. *Curr. Opin. Struct. Biol.* **1992**, *2*, 582–586.
(13) Chen, J. S.; Altman, G. H.; Karageorgiou, V.; Horan, R.; Collette, A.; Volloch, V.; Colabro, T.; Kaplan, D. L. *J. Biomed. Mater. Res.* **2003**, *67A*, 559–570.
(14) Meinel, L.; Karageorgiou, V.; Hofmann, S.; Fajardo, R.; Snyder, B.; Li, C.; Zichner, L.; Langer, R.; Vunjak-Novakovic, G.; Kaplan, D. L. *J Biomed. Mater. Res.* **2004**, *71A*, 25–34.
(15) Meinel, L.; Hofman, S.; Karageorgiou, V.; Kirker-Head, C.; McCool, J.; Gronowicz, G.; Zichner, L.; Langer, R.; Vunjak-Novakovic, G.; Kaplan, D. L. *Biomaterials* **2005**, *26*, 147–155.
(16) Gil, E. S.; Mandal, B. B.; Park, S.-H.; Marchant, J. K.; Omenetto, F. G.; Kaplan, D. L. *Biomaterials* **2010**, *31*, 8953–8963.
(17) Yao, J.; Asakura, T. In *Encyclopedia of Biomaterials and Biomedical Engineering*; Marcel Dekkers, Inc.: New York, 2004; pp 1363−1370.
(18) Asakura, T.; Tanaka, C.; Yang, M.; Yao, J.; Kurokawa, M. *Biomaterials* **2004**, *25*, 617–624.
(19) Yang, M.; Tanaka, C.; Yamauchi, K.; Ohgo, K.; Kurokawa, M.; Asakura, T. *J. Biomed. Mater. Res., Part A* **2008**, *84*, 353–363.
(20) Tanaka, C.; Asakura, T. *Biomacromolecules* **2009**, *10*, 923–928.
(21) Tamura, T.; Thilbert, C.; Royer, C.; Kanda, T.; Abraham, E.; Kamba, M.; Komoto, N.; Thomas, J. L.; Mauchamp, B.; Chavancy, G.; Shirk, P.; Fraser, M.; Prudhomme, J. C.; Couble, P. *Nat. Biotechnol.* **2000**, *18*, 81–84.
(22) Yanagisawa, S.; Zhu, Z.; Kobayashi, I.; Uchino, K.; Tamada, Y.; Tamura, T.; Asakura, T. *Biomacromolecules* **2007**, *8*, 3487–3492.
(23) Spitzfaden, C.; Grant, R. P.; Mardon, H. J.; Campbell, I. D. *J. Mol. Biol.* **1997**, *265*, 565–579.
(24) Copie, V.; Tomita, Y.; Akiyama, S. K.; Aota, S.; Yamada, K. M.; Venable, R. M.; Pastor, R. W.; Krueger, S.; Torchia, D. A. *J. Mol. Biol.* **1998**, *277*, 663–682.
(25) Saitô, H.; Tabeta, R.; Asakura, T.; Iwanaga, Y.; Shoji, A.; Ozaki, A.; Ando, I. *Macromolecules* **1984**, *17*, 1405–1412.
(26) Saitô, H. *Magn. Reson. Chem.* **1986**, *24*, 835–852.
(27) Asakura, T.; Ashida, J.; Yamane, T.; Kameda, T.; Nakazawa, Y.; Ohgo, K.; Komatsu, K. *J. Mol. Biol.* **2001**, *306*, 291–305.
(28) Asakura, T.; Yamane, T.; Nakazawa, Y.; Kameda, T.; Ando, K. *Biopolymers* **2001**, *58*, 521–525.
(29) Asakura, T.; Ohgo, K.; Komatsu, K.; Kanenari, M.; Okuyama, K. *Macromolecules* **2005**, *38*, 7397–7403.
(30) Asakura, T.; Yao, J. *Protein Sci.* **2002**, *11*, 2706–2713.
(31) Asakura, T.; Yao, J.; Yamane, T.; Umemura, K.; Ulrich, A. S. *J. Am. Chem. Soc.* **2002**, *124*, 8794–8795.
(32) Yang, Z. T.; Liivak, O.; Seidel, A.; LaVerde, G.; Zax, D. B.; Jelinski, L. W. *J. Am. Chem. Soc.* **2000**, *122*, 9019–9025.
(33) Suzuki, Y.; Aoki, A.; Nakazawa, Y.; Knight, D. P.; Asakura, T. *Macromolecules* **2010**, *43*, 9434–9440.
(34) Delaglio, F.; Grzesiek, S.; Vuister, G. W.; Zhu, G.; Pfeifer, J.; Bax, A. *J. Biomol. NMR* **1995**, *6*, 277–293.
(35) Goddard, T. D.; Kneller, D. G. *SPARKY 3*; University of California: San Francisco, CA; http://www.cgl.ucsf.edu/home/sparky/.
(36) Asakura, T.; Yoshimizu, H.; Yoshizawa, F. *Macromolecules* **1988**, *21*, 2038–2041.
(37) Le, H.; Oldfield, E. *J. Biomol. NMR* **1994**, *4*, 341–348.
(38) Asakura, T.; Taoka, K.; Demura, M.; Williamson, M. P. *J. Biomol. NMR* **1995**, *6*, 227–236.
(39) Spera, S.; Bax, A. *J. Am. Chem. Soc.* **1991**, *113*, 5490–5492.
(40) Asakura, T.; Iwadate, M.; Demura, M.; Williamson, M. P. *Int. J. Biol. Macromol.* **1999**, *24*, 167–171.